Growth mechanism for the controlled synthesis of MgH_2/Mg crystals via a vapor-solid process

Chunyu Zhu [†] Sou Hosokai, [†] Tomohiro Akiyama, [*†]

† Center for Advanced Research of Energy Conversion Materials, Hokkaido University, Sapporo 060-8628, Japan

* Corresponding author, Tel.: +81-11-706-6842; Fax: +81-11-726-0731.

Email: takiyama@eng.hokudai.ac.jp

ABSTRACT

In this paper, we continue the work on the controlled growth of MgH_2/Mg nano/microstructures, in which we highlight the growth mechanism from thermodynamics and kinetics, by a catalyst-free vapor-solid method of hydriding chemical vapor deposition (HCVD) which is a process of the evaporation-condensation of Mg under high-pressure H_2. We easily achieved control of both the morphology and composition, including nano/microsized powders of MgH_2 or a mixture of MgH_2 and Mg, nanosized straight and curved MgH_2 fibers, irregular bulk microstructures of Mg, hexagonal microplates of Mg, and microdendritic Mg, of the products by adjusting three experimental parameters: evaporation temperature, deposition temperature, and H_2 pressure. The products were compositionally separated into three categories, Mg, MgH_2, and a mixture of both, based on the growth temperature within the thermodynamic *P-T* diagram of the Mg-H system. A growth mechanism for the HCVD process was proposed from the perspectives of thermodynamics and kinetics, comprising a two-step reaction sequence on the deposition substrate of the first Mg condensation, $Mg_{(g)} \rightarrow Mg_{(s)}$, with subsequent hydrogenation, $Mg_{(s)} + H_{2(g)} \leftrightarrow MgH_{2(s)}$. The composition of the products was controlled by controlling the reaction rates of these two steps, in which these reaction rates were determined by the atmospheric conditions of deposition temperature, H_2 pressure and evaporation temperature. These Mg/MgH_2 nano/microstructures may find applications in hydrogen storage and batteries. By choosing suitable experimental parameters, such as evaporation temperature, deposition temperature, and H_2 pressure, this simple vapor-solid method may be extended to the synthesis of nano/microstructures of other metal hydrides.

KEYWORDS Hydrogen storage, magnesium hydride, nanostuctures, crystal growth, hydriding chemical vapor deposition

Introduction

Mg and MgH_2 are considerably attractive candidates for use in hydrogen storage as they can store a high H_2 content of theoretically up to 7.6 mass%; in Li-ion batteries, MgH_2 has a high theoretical electrical capacity of 2038 $Ah \cdot kg^{-1}$ as the negative electrode; and in metal-air batteries, Mg has a high theoretical voltage of 3.09 V and a high energy density up to 3910 $Wh \cdot kg^{-1}$.[1-3] The use of Mg in energy storage and conversion has many advantages, including its low cost, abundant resources, high energy density, and lack of toxicity to the environment. However, the practical use of MgH_2 or Mg in a hydrogen storage system for hydrogen-powered fuel cell vehicles has been impeded by the required high operation temperatures and the sluggish adsorption kinetics. Specifically, MgH_2 must be heated to ~300 ˚C to obtain a hydrogen equilibrium pressure of 1 bar; and to achieve a reasonable hydrogenation rate, a temperature of more than 400 ˚C is required. This is attributed to the high thermodynamic stability of MgH_2, which has a formation enthalpy of approximately -75 $kJ \cdot mol^{-1}$.[3,4] Nanostructuring of the material may be used to improve the hydrogen adsorption kinetics by increasing the specific surface area and number of grain boundaries, which shortens the reaction path and thus accelerates the diffusion rate through the solid phase.[5] Additionally, the reduced particle/grain size of MgH_2 minimizes the desorption energy of MgH_2, which decreases the desorption temperature.[6] Further, in order to use MgH_2 or Mg as the electrode material in Li-ion or metal-air batteries, downsized material is required to obtain the required high charging/discharging rates and conversion efficiencies.[1,2]

To obtain a destabilized MgH_2 or Mg with a lowered operation temperature and enhanced H_2 adsorption kinetics, a number of efforts have been made to manufacture nano/microsized MgH_2 or Mg and their composites, such as ball-milling of Mg or MgH_2 and their composites,[7,8] infiltration of nanoporous carbon with molten magnesium,[9] electrochemical synthesis of colloidal Mg nanoparticles,[10] physical vapor transport deposition (PVD) of Mg nanowires,[11] and hydriding chemical vapor deposition (HCVD) of MgH_2 nanofibers[12-15]. Among these, HCVD is a promising method that uses the condensation of gasified Mg under a high pressure H_2 atmosphere, which is a vapor-solid crystal growth process, to synthesize MgH_2/Mg nano/microstructures with a controllable growth.[13] The HCVD method has many benefits for producing MgH_2: it can produce MgH_2 at a low cost by using waste Mg as the raw material,[16] it offers a controllable high-purity product, and it minimizes the production energy, shortens the operating time, and enables control over the growth of the nano/microsized structures.

The growth of crystals from vapor is controlled through the atmospheric conditions. Historically, Dr. Ukichiro Nakaya of Hokkaido University, Sapporo, is famous for publishing his Nakaya Diagram, which describes the relationship between the growth of snow crystals and the atmospheric conditions of temperature and supersaturation. This diagram allows us to "read" the meteorological information "written" on snow crystals, which are “letters sent from heaven”.[17] From the perspective of “everything can be snow”, the controlled growth of MgH_2/Mg crystals under controllable atmospheric conditions is of considerable interest to researchers in the fields of crystal growth, material synthesis, chemical engineering, hydrogen storage and batteries. For the vapor-solid growth of snow crystals, the system comprises only one component (H_2O) and two phases (vapor and solid crystal); the process of the evaporation of H_2O vapor from liquid water is neglected. However, for the vapor-solid growth of MgH_2/Mg from gasified Mg under an H_2 atmosphere, this system contains three components (H_2, Mg, and MgH_2), with two phases (vapor and solid crystal), which makes the growth process quite complex. In our recent studies, various MgH_2/Mg structures have been produced by changing the growth temperature and H_2 pressure at a fixed evaporation temperature.[13,14] However, for this three-component and two-phase HCVD process, the growth process would be affected by the deposition temperature, H_2 pressure, and Mg vapor partial pressure as well as the thermodynamic properties of MgH_2 and the hydrogenation kinetics of Mg. All of these factors play an important role in the morphology and composition of the product. Further, the growth mechanism underlying the HCVD process is still unclear, although it must be influenced by the atmospheric conditions as well as the thermodynamics and hydrogenation kinetics for MgH_2 formation.

Herein, using the simple vapor-solid crystal growth method via the HCVD process with a modified apparatus, we report the controlled synthesis and growth mechanism of MgH_2/Mg nano/microstructures. We were able to control the morphologies, including fine and coarse powders, straight and curved fibers, irregular bulk structures, hexagonal plates, and microdendrites, and compositions of the nano/microsized MgH_2/Mg products by changing the substrate temperature, H_2 pressure, and the Mg vapor concentration, which is determined by the evaporation temperature and H_2 pressure. A two-step reaction mechanism for the first Mg vapor condensation with subsequent hydrogenation of the solidified Mg on the substrate for the growth of MgH_2 or Mg is proposed, whereas the composition of the product is determined by the thermodynamics of the Mg-H system and the hydrogenation kinetics of Mg.

Experimental section

MgH_2/Mg nano/microstructures were produced via the hydriding chemical vapor deposition (HCVD) method.[12-14] The same experimental setup was used as that described by Zhu et al.[13] To evaluate the effect of the evaporation temperature under various H_2 pressures on the growth of MgH_2/Mg crystals, the apparatus was modified to allow a maximum working temperature of 700 ˚C under an H_2 pressure of < 2.2 MPa. A piece of stainless steel mesh (1000 mesh, SEM image of the mesh is shown in Figure S1, Supporting Information) was adhered to the tube wall of the reactor and used as the substrate to collect the products. The temperature distribution along the inner top of the tube wall with the mesh on was measured before the experiment under 1 and 2 MPa of H_2 with evaporation temperatures of 600, 650, and 700 ˚C; the results are shown in Figures S2 and S3 in the Supporting Information.

Five grams of raw Mg (purity 99.9%, particle size < 75 μm) were heated to vaporization at temperatures of 600, 650, and 700 ˚C under H_2 (purity of 99.99999%) pressures of 1 and 2 MPa for 4 h. The H_2 and Mg vapor reactants were deposited onto the cooled substrate and to form the MgH_2/Mg products. Deposits with widths of 2 cm on the mesh near the inner top portion of the tube wall were collected for characterization.

The obtained samples were characterized by powder X-ray diffraction (XRD, Rigaku Miniflex, CuKα) for composition analysis and scanning electron microscopy (SEM, JEOL, JSM-6360LA) for morphology observation.

Results and discussion

Controlled growth of MgH_2/Mg nano/microstructures

MgH_2/Mg nano/microstructures were synthesized via the HCVD method using a variety of H_2 pressures, deposition temperatures, and evaporation temperatures. Figure 1 shows the images of the products, which were obtained at evaporation temperatures of 600, 650, and 700 ˚C under H_2 pressures of either 1 or 2 MPa, deposited on the mesh substrate at a temperature ranging from ~300 ˚C to ~500-650 ˚C. The as-measured dissociation temperatures are indicated by the red solid lines in Figure 1. These temperatures act as the boundaries that separate the MgH_2 and Mg stable areas since MgH_2 decomposes to form Mg and H_2 at temperatures above the dissociation temperatures of MgH_2 under 1 and 2 MPa H_2. The measured dissociation temperatures in this study disagree with the theoretical ones, which tend to be at higher temperatures; this shift is mainly due to the fluctuation of the temperature distribution caused by the H_2 convention, which was reported in our previous study.[13]

SEM was used to observe the micromorphology of the deposits, which were obtained at varying evaporation and deposition temperatures under H_2 pressures of either 1 or 2 MPa. The SEM images for the deposits obtained at the different deposition conditions are shown in Figure 1. More details about the product images and micromorphology can be found in Supporting Information, Figures S2 and S3. At the temperatures above the boundary temperatures of dissociation, the deposits are metallic and shiny, which were confirmed to be Mg by XRD analysis. These metallic Mg deposits show irregular bulk, hexagonal and dendritic or large plate shapes at the microscale. The hexagonal and dendritic deposits were obtained at higher temperature zones than the irregular shapes. Also, the dendritic deposits were obtained with higher evaporation temperatures of 650 and 700 ˚C, where the Mg vapor concentration is high. Below the boundary temperatures and under 1 MPa of H_2 pressure, powder-shaped crystals of the nano- and microscale were deposited; the powders were finer at lower temperatures than that at high temperatures. At evaporation temperatures of 600 and 650 ˚C, a few straight fine fibers were deposited with the root-like and curved coarse fibers, which were mixed with the big powders at deposition temperatures near the dissociation temperatures. At 2 MPa of H_2 pressure with an evaporation temperature of 700 ˚C, only powder-shaped crystals were deposited; however, at evaporation temperatures of 650 and 600 ˚C, fine powders, coarse powders, root-like, curved coarse fibers, and straight fine fibers were produced as the deposition temperature increased from low to high. The fibers obtained at an evaporation temperature of 600 ˚C were straighter and finer than those produced at 650 ˚C. In

conclusion, the size and morphology of the deposits are quite dependent on the growth conditions including deposition temperature, H_2 pressure, and evaporation temperature (which determines the Mg gas concentration).

XRD was used to analyze the phase composition of the products. The inserted numbers S1, S2, S3 etc. in Figure 1 indicate the sample preparation method. Figure 2 shows the XRD patterns of the products obtained at varying evaporation temperature and deposition temperature areas under H_2 pressures of 1 and 2 MPa. At the temperatures above the boundary temperatures of dissociation, metallic Mg was deposited. The weak peaks corresponding to MgH_2 in samples S4, S5, S6, and S7 were formed during the cooling process after 4 h of growth at a constant H_2 pressure; similar phenomena were found in our previous study.[13] The peaks corresponding to metallic Mg shift in their preferred orientation from Mg (101) to Mg (002) as the deposition temperature increased. The preferred orientation is consistent with the microstructure of the deposited crystals; powder-shaped and irregular bulk deposits have a (101) preferred face, and hexagonal and dendritic plates have a preferred orientation of (001). Below the boundary temperatures is the MgH_2 stable area where only MgH_2 should be produced from a thermodynamic perspective; however, the products obtained at the lower temperatures, especially those produced at higher evaporation temperatures and lower H_2 pressures, were incompletely hydrogenated metallic Mg. This is due to the low hydrogenation rate for Mg at lower temperatures and H_2 pressures; more about this will be presented in the growth mechanism section below.

On the basis of the XRD composition analysis, the blue lines in Figure 1 enclose the three product areas: (1) mixtures of MgH_2 and Mg, (2) highly pure MgH_2, and (3) metallic Mg. Figure 3 features the thermodynamic *P*-*T* diagram of MgH_2, which summarizes the boundaries for separating the high-purity-MgH_2 and low-purity-MgH_2 production areas with evaporation temperatures of 600, 650, and 700 ˚C, as well as the experimentally measured boundary for the thermodynamically MgH_2 and Mg stable areas.

Growth mechanism

Crystal growth is a heterogeneous or homogeneous chemical process involving the use of solids, liquids, or gases, either individually or together, to form a homogeneous solid substance with a three-dimensional atomic arrangement. Various processes and techniques have been employed for crystal growth depending upon the chemical processes involved and can be broadly classified into three categories: solid → solid, liquid → solid, and vapor → solid, according to the Handbook of Crystal Growth.[18] Here, the HCVD process involves the

crystal growth from a vapor to a solid using a sublimation-condensation process, which primarily involves three stages: (1) vaporization, (2) transportation, and (3) deposition.

Growth steps in the HCVD process: Figure 4 shows the sequence of steps in the HCVD process. The HCVD process contains the following detailed steps from the evaporation region to the deposition region:

(1) Evaporation of raw Mg under high-pressure H_2 atmosphere in the hot region.

(2) Transfer of Mg gas by natural convection and diffusion of H_2 induced by the temperature gradient from the hot zone to the cooled zone.

(3) Adsorption and condensation of Mg gas on the surface of the cooled substrate or the already formed deposits.

(4) Adsorption and dissociation of H_2 molecules on the surface of the cooled substrates or the already formed deposits.

(5) Formation of MgH_2 by the hydrogenation of the adsorbed and solidified Mg on the substrate at temperatures below the dissociation temperature of MgH_2 under a certain H_2 pressure. Above the dissociation temperature, only metallic Mg is formed. At very low deposition temperatures, the hydrogenation rate for the solidified Mg is slow, and the deposit contains unhydrogenated Mg.

In the HCVD process for the growth of MgH_2 or Mg, the Mg raw material is first gasified in the hot region in a closed system with temperatures of 600–700 ˚C under a high-pressure (> 1 MPa) H_2 atmosphere. The vaporized Mg is then transported to the cool zone by natural convection and diffusion of H_2, which is caused by a temperature gradient, to form MgH_2 or Mg crystals on the cooled substrate. The HCVD process can be represented by a simple reaction sequence as follows:

$$Mg_{(s)} \xrightarrow{\text{hot zone: evaporation at high pressure } H_2} Mg_{(g)} \xrightarrow{\text{transportation}} \xrightarrow{\text{cooled zone: deposition at high pressure } H_2} MgH_{2(s)} \text{ or } Mg_{(s)}$$

The HCVD growth process for MgH_2 or Mg crystals is quite similar to the physical vapor transport (PVT) process for AlN bulk crystal growth.[19] In a typical PVT process an AlN powder source is sublimed at high temperatures (> 2000 ˚C) within a closed or semiopen crucible. The vapors are then transported in a nitrogen atmosphere or vacuum under atmospheric or very low pressure through a temperature gradient to a region held at a lower temperature than the source, where they recrystallize. The PVT growth process of AlN can be represented by the following reaction sequence, which is modified from a study by Epelbaum

et al.:[20]

$$AlN_{(s)} \xrightarrow{\text{hot zone: evaporation}} Al_{(g)} + 0.5N_{2(g)} \xrightarrow{\text{transportation}} \xrightarrow{\text{cooled zone: deposition}} AlN_{(s)}$$

Both of these processes utilize sublimed metals, which are transported to a cooled substrate for recrystallization. The differences between these two processes are as follows: the PVT process uses a low pressure N_2 atmosphere with only one deposit of AlN, while the HCVD process requires a high pressure of H_2, and the deposits are either MgH_2, or Mg, or a mixture of both. For HCVD, the type of deposit depends on the growth temperature and H_2 pressure; the products are separate due to the thermodynamic properties of MgH_2. Specifically, MgH_2 decomposes at temperatures above the dissociation temperature under certain H_2 pressures, and a high H_2 pressure is necessary for the hydrogenation reaction of Mg.

The entire HCVD process is under a high-pressure H_2 atmosphere with a total pressure of $P_{total} = P_{Mg} + P_{H_2}$; P_{total} = 1, 2, 3, or 4 MPa $\approx P_{H_2} >> P_{Mg}$. The total pressure is kept constant by adding H_2, which leads to the Mg vapor becoming a minor component. Therefore, it is reasonable to assume that P_{Mg} limits the global rate for MgH_2 or Mg deposition. In this work, utilizing thermodynamics and kinetics, we concentrate on the steps of Mg evaporation in the hot region and the deposition of MgH_2 or Mg on the cooled substrate. The simulation of the vapor transportation effect is beyond the ability of this study, as in the present study the transportation of vapor is driven by natural convection and diffusion of H_2 caused by a temperature gradient.

Effect of the evaporation temperature (reactions in the hot region): In the hot zone, the Mg raw material is vaporized at high temperatures; the Mg gas concentration is influenced by the evaporation temperature as well as the H_2 pressure. The theoretical Mg gas partial pressure can be determined from the equilibrium of the following two reactions:

$$Mg_{(s)} \leftrightarrow Mg_{(g)} \qquad K_1 = P_{Mg_{(g)}} \qquad (1)$$

$$Mg_{(s)} + H_{2(g)} \leftrightarrow MgH_{2(s)} \qquad K_2 = 1 / P_{H_2} \qquad (2)$$

where K_1 and K_2 are the reaction equilibrium constants for these two reactions. The equilibrium vapor partial pressures of Mg under H_2 pressures of 1, 2, 3, and 4 MPa as a function of temperature are calculated using HSC Chemistry software (version 5.1) and are

presented in Figure 5. From this figure we can confirm that (1) with increasing evaporation temperature, the Mg gas concentration increases dramatically, leading to higher supersaturation degree in the gas phase which is the driving force for Mg condensation; (2) the equilibrium Mg partial pressure is significantly influenced by the H_2 or total pressure, since Mg sublimes more easily at a low H_2 pressure. A high Mg vapor concentration gives a high supersaturation driving force in the deposition area, which leads to a high growth rate of MgH_2 or Mg deposits. However, the formation of MgH_2 is complexly influenced by the thermodynamics of the Mg-H system and the kinetics of the hydrogenation reaction of solid Mg. These effects are discussed in the following section.

Reactions in the deposition area: For the condensation of Mg gas to form MgH_2 on the cooled substrate, we can speculate on possible individual reaction steps using a Hertz-Knudsen adsorption model, which has been used to describe the PVT growth process of AlN.[20] The proposed steps are as follows:

$$Mg_{(g)} \leftrightarrow Mg_{ads} \quad (3)$$

$$Mg_{ads} \leftrightarrow Mg_{(s)} \quad (4)$$

$$H_{2(g)} \leftrightarrow H_{2\ ads} \quad (5)$$

$$H_{2\ ads} \leftrightarrow 2H_{ads} \quad (6)$$

$$Mg_{ads} + 2H_{ads} \leftrightarrow MgH_{2(s)} \quad (7)$$

$$Mg_{ads} + H_{2\ ads} \leftrightarrow MgH_{2(s)} \quad (8)$$

$$Mg_{(s)} + 2H_{ads} \leftrightarrow MgH_{2(s)} \quad (9)$$

$$Mg_{(s)} + H_{2\ ads} \leftrightarrow MgH_{2(s)} \quad (10)$$

Equations (3) and (4) represent the adsorption and condensation, respectively, of Mg vapor to form solid Mg on the substrate according to step (3) in Figure 4. Equations (5) and (6) show the adsorption and dissociation of H_2 molecules to H atoms, respectively, on the surface of the substrate or the already formed deposits according to step (4) in Figure 4. Equations (7)−(10) describe the hydrogenation steps for the formation of MgH_2, as shown by step (5) in Figure 4.

It is difficult to measure the condensation coefficient, α, and reaction rate for each species and reaction that appear in the above formulas. Therefore, for simplicity, two reactions in the series are proposed for the formation of MgH_2 on the cooled substrate during the HCVD process:

$$Mg_{(g)} \rightarrow Mg_{(s)} \quad R_1 \quad (11)$$

$$Mg_{(s)} + H_{2(g)} \leftrightarrow MgH_{2(s)} \qquad R_2 \qquad (12)$$

where R_1 and R_2 are the reaction rates for Eqs. (11) and (12), respectively. From this two-step reaction, we can conclude that the composition of the deposits is controlled by the balance of the reaction rates for Eqs. (11) and (12). The reaction represented by Eq. (11) is the solidification of gasified Mg, for which the growth driving force is supersaturation, which is determined by the Mg gas concentration and the deposition temperature; a high Mg gas concentration and low deposition temperature give a high rate for the condensation of Mg vapor. The reaction as shown in Eq. (12), which is the hydrogenation of solidified Mg, has a high reaction rate under high H_2 pressures and growth temperatures in the MgH_2 stable area of the MgH_2 *P-T* diagram. Here, the hydrogenation reaction does not occur at temperatures higher than the thermodynamic dissociation temperatures of MgH_2 at certain H_2 pressures within the Mg stable area in the *P-T* diagram of MgH_2 and MgH_2 decomposes thermodynamically, in which $R_1 >> R_2$ and only Mg deposits are obtained. At temperature areas lower than the thermodynamic dissociation temperatures of MgH_2 at certain H_2 pressures, that is within the MgH_2 stable area of the *P-T* diagram of MgH_2, there are two potential situations: (1) at higher temperatures, especially at a high H_2 pressure with a lower evaporation temperature (this means a low Mg concentration), near the dissociation temperature, high-purity MgH_2 is produced, and the hydrogenation rate is larger than the Mg solidification rate, $R_2 > R_1$; (2) at lower temperatures, especially at low H_2 pressures with a high evaporation temperature (this means a high Mg concentrations), beyond the dissociation temperature, a mixture of MgH_2 and Mg is obtained, unhydrogenated Mg accumulates, and the hydrogenation rate is smaller than the Mg solidification rate, $R_2 < R_1$. These conclusions have been proven by the experimental results in this work and our previous study.[13]

A vapor-solid (V-S) growth mechanism was introduced in our previous studies [13,14] to explain the HCVD crystal growth because no catalyst was used in the growth process. In this work, we numerically demonstrate the growth process based on this two-step reaction on the deposition substrate.

The first step of Mg condensation: The reaction rate for the first step of condensation of the vaporized Mg can be derived from the Hertz-Knudsen formula, which is modified from a paper by Irisawa:[21]

$$R_1 = \frac{\alpha V_a (p - p_e)}{\sqrt{2\pi m k_B T}} = C\frac{p - p_e}{\sqrt{T}}; \quad C = \frac{\alpha V_a}{\sqrt{2\pi m k_B}} = const.$$

where α is the condensation coefficient, V_a is the atomic volume, m is the mass of an Mg atom, k_B is Boltzmann's constant, T is temperature, p is the real vapor pressure, and p_e is the equilibrium vapor pressure at a given temperature, T, for Mg. It must be noted that the growth rate calculated using this formula is proportional to the supersaturation, p-p_e, at a given temperature, which is the growth driving force for condensation. The growth rates for Mg condensation at different evaporation temperatures and H_2 pressures of 1 and 2 MPa as a function of deposition temperature are represented by the solid lines in Figure 6; red lines for 1 MPa, and blue lines for 2 MPa.

The second step of hydrogenation: The formation of MgH_2 is a heterogeneous phase transformation process in which solid Mg combines with H_2 to produce MgH_2, which is referred to as hydrogenation. The hydrogenation process comprises a series of steps: absorption and dissociation of H_2 molecules on the surface, surface penetration of hydrogen atoms, H diffusion through the hydride layer, and hydride formation at the metal/hydride interface.[22,23] The slowest of these is the rate-limiting step for the formation of MgH_2 by the hydrogenation of solid Mg.

In a typical kinetic experiment for the hydrogenation of solid Mg, the absorption experiment of the gas-solid reaction is represented by the reacted fraction, r_f, which is recorded as a function of time, t, sample temperature, T, H_2 pressure, P, and for different sample shapes, s. In most cases the relationship between all these parameters can be presented in a simple form:[23]

$$F(r_f) \propto k(P, T, s) \cdot t$$

The function, F, depends on the controlling mechanism of the reaction, whereas the parameter k determines the reaction rate, which depends on the P, T, and sample shape. Therefore, the reaction rate of k can be expressed as a function of these three parameters:

$$k(P, T, s) \propto f(s) \cdot g(P/P_{eq}) \cdot h(T)$$

where $f(s)$ is related to the sample geometry, $g(P/P_{eq})$ is the driving force for hydrogenation, and $h(T)$ can be represented by the Arrhenius Equation, which describes the dependence of the

rate constant on the absolute temperature, T:

$$h(T) = k_0 \exp(-E_a/RT)$$

where k_0 is the pre-exponential factor, E_a is the activation energy for the overall reaction, and R is the gas constant.

In this study, the reality for the second step of hydrogenation of the solidified Mg on the cooled substrate is that the hydrogenation reaction takes place along with the condensation of Mg. Specifically, very small Mg nucleus combines with H_2 to form MgH_2 after which the crystal grows bigger as condensation proceeds with subsequent hydrogenation taking place on the surface of the deposits. Therefore, the effect of geometry on the overall hydrogenation rate can be neglected in this study because the hydrogenation reaction always occurs on the surface of the deposits with a very short hydrogen diffusion path. Note that, at very low deposition temperatures, the production area of a mixture of MgH_2 and Mg, in which the hydrogenation rate is slower than the condensation rate, a step involving hydrogen diffusion to the inner portion of the deposit is needed since the core of the deposit is only partly hydrogenated.

In summary, the reaction rate, R_2, for the hydrogenation step in the HCVD process can be represented as:

$$\begin{aligned} R_2 &\propto g(P/P_{eq}) \cdot h(T) \\ &\propto g(P/P_{eq}) \cdot (k_0 \exp(-E_a/RT)) \end{aligned}$$

From this equation we can confirm that the reaction rate for hydrogenation is influenced by both the H_2 pressure and growth temperature; a high H_2 pressure and high temperature in the MgH_2 stable area result in high hydrogenation kinetics; and the curve of R_2 satisfies an exponential function versus temperature under a certain H_2 pressure.

In Figure 6, the reaction rate, R_2, of the hydrogenation step as a function of temperature is plotted as the dash-dot lines under H_2 pressures of 1 and 2 MPa, which is based on the boundary temperatures that separate the production areas for high-purity MgH_2 and mixtures of both MgH_2 and Mg in the thermodynamically MgH_2 stable area, as shown in Figures 1, 2, and 3.

From Figure 6, we can confirm that (1) above the dissociation temperature at a certain H_2 pressure, only Mg deposits are obtained; (2) below the dissociation temperature, when $R_2 > R_1$

high-purity MgH_2 is produced, and when $R_1 > R_2$ a mixture of MgH_2 and Mg is obtained; (3) a high H_2 pressure offers a larger high-purity MgH_2 production area; and (4) the composition of the products under other growth conditions can be predicted using this figure, e.g., by increasing the H_2 pressure the theoretical dissociation temperature shifts to high temperatures and the hydrogenation rate also increases, in which the boundaries for separating the production areas for high-purity MgH_2 and mixtures of both MgH_2 and Mg shift to low temperatures, then the high-purity MgH_2 production area enlarges, and vice versa. A thorough explanation of this Figure 6 is shown in Figure S4 in the Supporting Information.

Conclusions

In conclusion, we carried out the controlled synthesis of MgH_2/Mg nano/microsturctures via hydriding chemical vapor deposition (HCVD). In the synthesis, different concentrations of Mg vapor, which was obtained by varying the evaporation temperatures at 600, 650, and 700 ˚C under H_2 pressures of 1 and 2 MPa, were deposited on a stainless steel substrate at temperatures ranging from ~300–600 ˚C. The deposits obtained after a growth time of 4 h were identified by X-ray diffraction and observed by scanning electron microscopy. The composition, morphology, and size of the products strongly depended on the experimental conditions, which were controlled by changing the deposition temperature, H_2 pressure, and evaporation temperature based on the thermodynamics and kinetics of the Mg-H system. Fine and coarse powders, straight and curved fibers, irregular bulk structures, hexagonal plates, and microdendrites were obtained under different growth conditions. The products were compositionally separated into three areas (Mg, MgH_2, and a mixture of both) based on the growth temperature within the thermodynamic *P-T* diagram of the Mg-H system. A growth mechanism for the HCVD process was proposed, and a two-step reaction sequence on the deposition substrate of first Mg condensation ($Mg_{(g)} \rightarrow Mg_{(s)}$) with subsequent hydrogenation ($Mg_{(s)} + H_{2(g)} \leftrightarrow MgH_{2(s)}$) was introduced; the composition of the product was controlled by the reaction rates of these two steps.

Hydriding chemical vapor deposition has many advantages for the production of MgH_2/Mg: it offers a product with controllable composition, it enables control over the growth of nano/microsized structures, and it can produce MgH_2 at a low cost using waste Mg as the raw material for this evaporation-condensation method with minimized energy consumption. These Mg/MgH_2 structures may find applications in hydrogen storage and batteries. By choosing suitable experimental parameters, such as evaporation temperature, deposition temperature, and H_2 pressure, this simple vapor-solid method may be extended to synthesize nano/microstructures of other metal hydrides.

Supporting Information Available: (1) Figure S1: The enlarged image of the mesh (SUS316) used to collect the products. (2) Figure S2: The product images, temperature distribution, and SEM images under 1 MPa H_2. (3) Figure S3: The product images, temperature distribution, and SEM images under 2 MPa H_2. (4) Figure S4: Mg gas condensation rate and the hydrogenation rate for solidified Mg at 1 and 2 MPa H_2, respectively. This information is available free of charge via the Internet at http://pubs.acs.org/.

Reference

(1) Oumellal, Y.; Rougier, A.; Nazri, G. A.; Tarascon, J. M.; Aymard, L. *Nat. Mater.* **2008**, *7*, 916.

(2) Li, W. Y.; Li, C. S.; Zhou, C. Y.; Ma, H.; Chen, J. *Angew. Chem. Int. Ed.* **2006**, *45*, 6009.

(3) Schlapbach, L.; Zuttel, A. *Nature* **2001**, *414*, 353.

(4) Aguey-Zinsou, K. F.; Ares-Fernandez, J. R. *Energy Environ. Sci.* **2010**, *3*, 526.

(5) Zaluska, A.; Zaluski, L.; Ström-Olsen, J. O. *J. Alloys and Compd.* **1999**, *288*, 217.

(6) Wagemans, R. W. P.; van Lenthe, J. H.; de Jongh, P. E.; van Dillen, A. J.; de Jong, K. P. *J. Am. Chem. Soc.* **2005**, *127*, 16675.

(7) Varin, R. A.; Czujko, T.; Wronski, Z. *Nanotechnology* **2006**, *17*, 3856.

(8) Lu, J.; Choi, Y. J.; Fang, Z. Z.; Sohn, H. Y.; Rönnebro, E. *J. Am. Chem. Soc.* **2010**, *132*, 6616.

(9) Jongh, P. E. d.; Wagemans, R. W. P.; Eggenhuisen, T. M.; Dauvillier, B. S.; Radstake, P. B.; Meeldijk, J. D.; Geus, J. W.; Jong, K. P. d. *Chem. Mater.* **2007**, *19*, 6052.

(10) Aguey-Zinsou, K. F.; Ares-Fernandez, J. R. *Chem. Mater.* **2008**, *20*, 376.

(11) Li, W. Y.; Li, C. S.; Ma, H.; Chen, J. *J. Am. Chem. Soc.* **2007**, *129*, 6710.

(12) Saita, I.; Toshima, T.; Tanda, S.; Akiyama, T. *Mater. Trans.* **2006**, *47*, 931.

(13) Zhu, C.; Hosokai, S.; Matsumoto, I.; Akiyama, T. *Cryst. Growth Des.* **2010**, *10*, 5123.

(14) Zhu, C.; Hayashi, H.; Saita, I.; Akiyama, T. *Int. J. Hydrogen Energy* **2009**, *34*, 7283.

(15) Zhu, C.; Sakaguchi, N.; Hosokai, S.; Watanabe, S.; Akiyama, T. *Int. J. Hydrogen Energy* **2011**, *36*, 3600.

(16) Zhu, C.; Hosokai, S.; Akiyama, T. Mg recycling with production of MgH_2 nanofibers using hydriding chemical vapor deposition. Paper in preparation.

(17) Nakaya U. Snow Crystals, Natural and Artificial. Cambridge: Harvard Univ. Press; 1954.

(18) Govindhan Dhanaraj, Kullaiah Byrappa, Vishwanath Prasad, and Michael Dudley (Eds.), Springer Handbook of Crystal Growth, 2010; Part A - Fundamentals of Crystal Growth and Defect Formation; Chapter 1 - Crystal Growth Techniques and Characterization: An Overview - by Govindhan Dhanaraj, Kullaiah Byrappa, Vishwanath (Vish) Prasad, and Michael Dudley.

(19) Govindhan Dhanaraj, Kullaiah Byrappa, Vishwanath Prasad, Michael Dudley (Eds.), Springer Handbook of Crystal Growth, 2010; Part D - Crystal Growth from Vapor; Chapter 24 - AlN Bulk Crystal Growth by Physical Vapor Transport - by Rafael Dalmau and Zlatko Sitar.

(20) Epelbaum, B. M.; Bickermann, M.; Winnacker, A.; Trans Tech Publ: 2004; Vol. 457, p 1537.

(21) K. Byrappa and T. Ohachi (Eds.), Crystal Growth Technology,Springer 2003; Chapter 2 - Theory of Crystal Growth from Vapor and Solution - by Toshiharu Irisawa.

(22) Martin, M.; Gommel, C.; Borkhart, C.; Fromm, E. *J. Alloys Compd.* **1996**, *238*, 193.

(23) Fernandez, J. F.; Sanchez, C. R. *J. Alloys Compd.* **2002**, *340*, 189.

For Table of Contents Use Only

Controlled growth, both in morphology and composition, of MgH_2/Mg nano/microstructures via a catalyst-free vapor-solid method of hydriding chemical vapor deposition (HCVD) which is a process of the evaporation-condensation of Mg under a high H_2 pressure, was achieved by adjusting the evaporation temperature, deposition temperature and H_2 pressure. The growth mechanism was highlighted from the aspects of thermodynamics and kinetics for the Mg-H system.

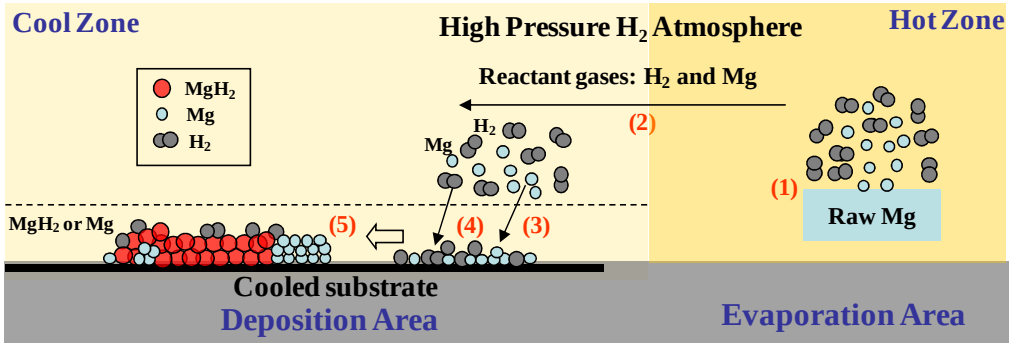

Figure 1

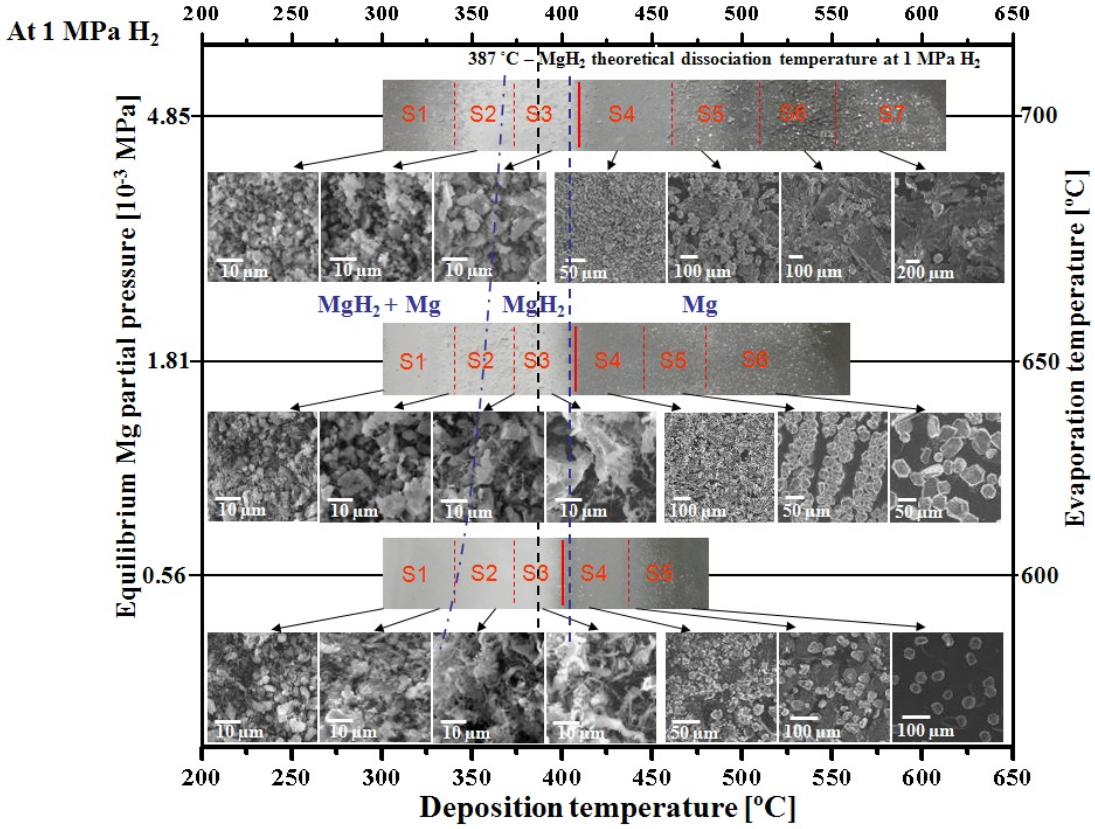
At 1 MPa H_2
387 °C – MgH_2 theoretical dissociation temperature at 1 MPa H_2
S1
S2
S3
S4
S5
S6
S7
4.85
1.81
0.56
700
650
600
MgH_2 + Mg
MgH_2
Mg
Equilibrium Mg partial pressure [10^{-3} MPa]
Evaporation temperature [°C]
Deposition temperature [°C]
200
250
300
350
400
450
500
550
600
650

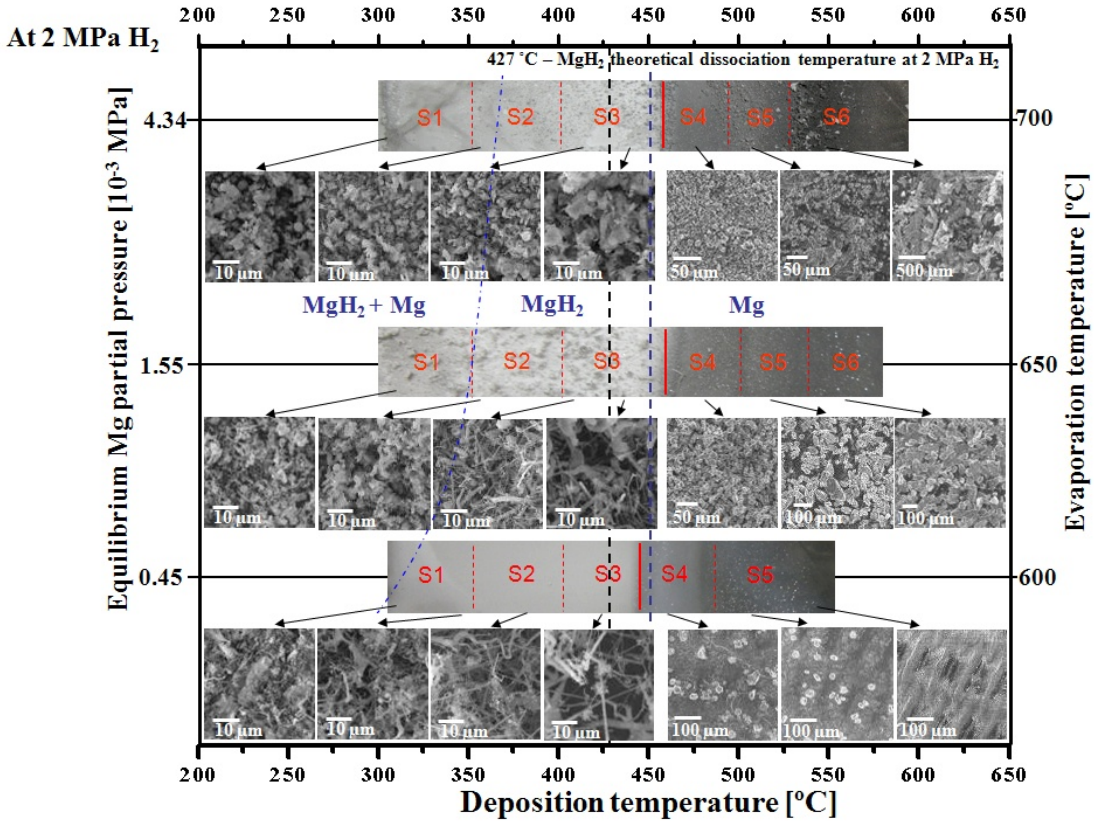
At 2 MPa H_2
427 °C – MgH_2 theoretical dissociation temperature at 2 MPa H_2
S1
S2
S3
S4
S5
S6
4.34
1.55
0.45
700
650
600
MgH_2 + Mg
MgH_2
Mg
Equilibrium Mg partial pressure [10^{-3} MPa]
Evaporation temperature [°C]
Deposition temperature [°C]
200
250
300
350
400
450
500
550
600
650

Figure 1. The images and micro-morphology of the deposits at different deposition temperatures obtained at evaporation temperatures of 600, 650, and 700 ˚C, which were prepared under 1 and 2 MPa H_2 atmosphere, respectively. These images were edited to adjust the temperature distribution. The red solid lines indicate the as-measured dissociation temperatures of MgH_2 under 1 and 2 MPa H_2 in this study as compared with the theoretical dissociation temperatures. The inserted numbers S1, S2, S3 etc. were used for XRD sample preparation, as shown in Figure 2. (For more details about the product images and micro-morphology, see Supporting Information, Figures S2 and S3). An evaporation time of 4 h was used for each batch of experiment. The calculation for the equilibrium Mg partial pressure at varying evaporation temperatures and H_2 pressures is shown in Figure 5. The two blue lines in each figure roughly separate the three product areas of Mg, MgH_2, and a mixture of both based on the XRD composition analysis in Figure 2.

Figure 2

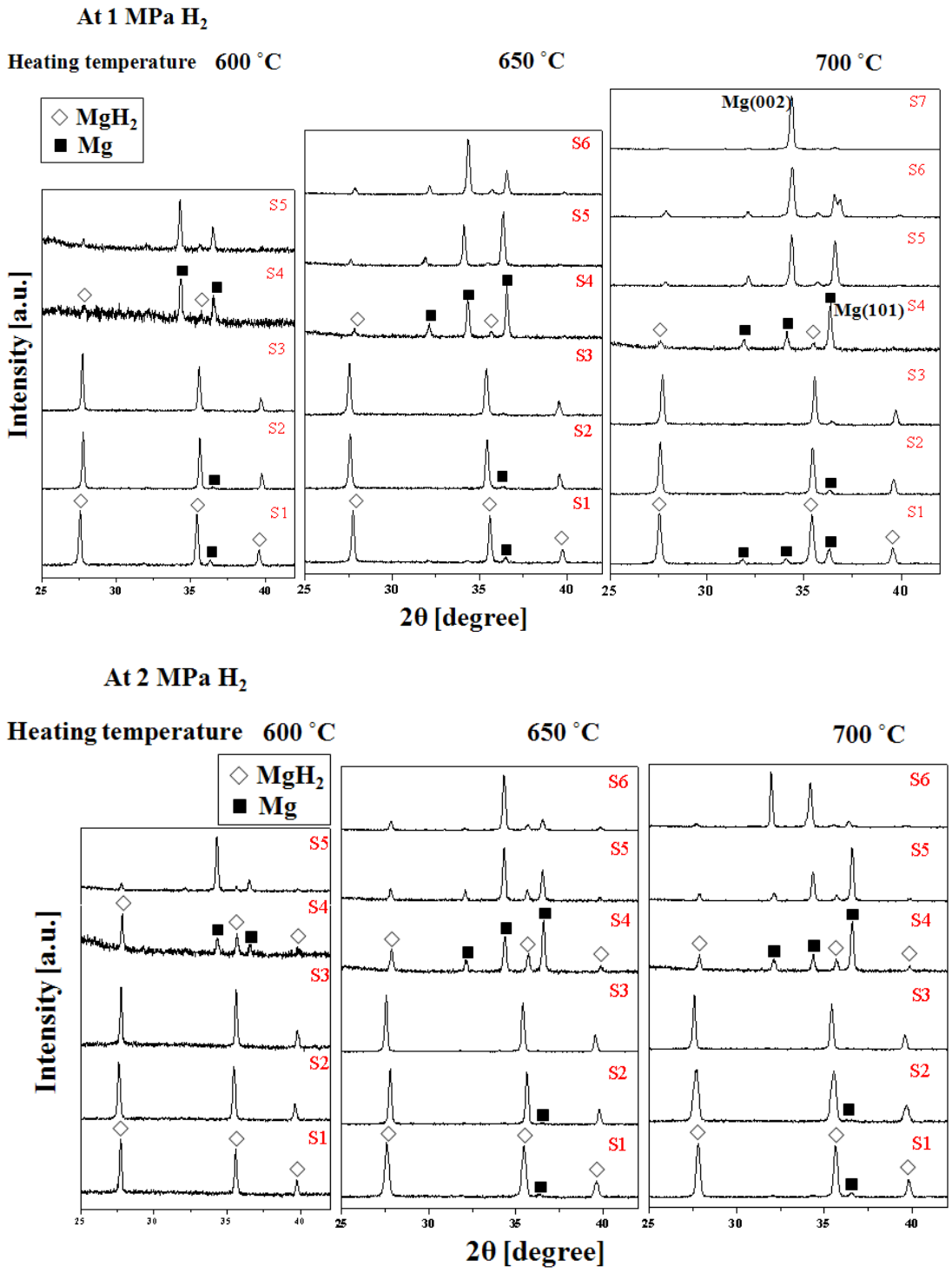

Figure 2. XRD patterns of the samples obtained at different deposition temperature areas under 1 and 2 MPa of H_2 at evaporation temperatures of 600, 650 and 700 ˚C. The sample numbers correspond to those in Figure 1.

Figure 3

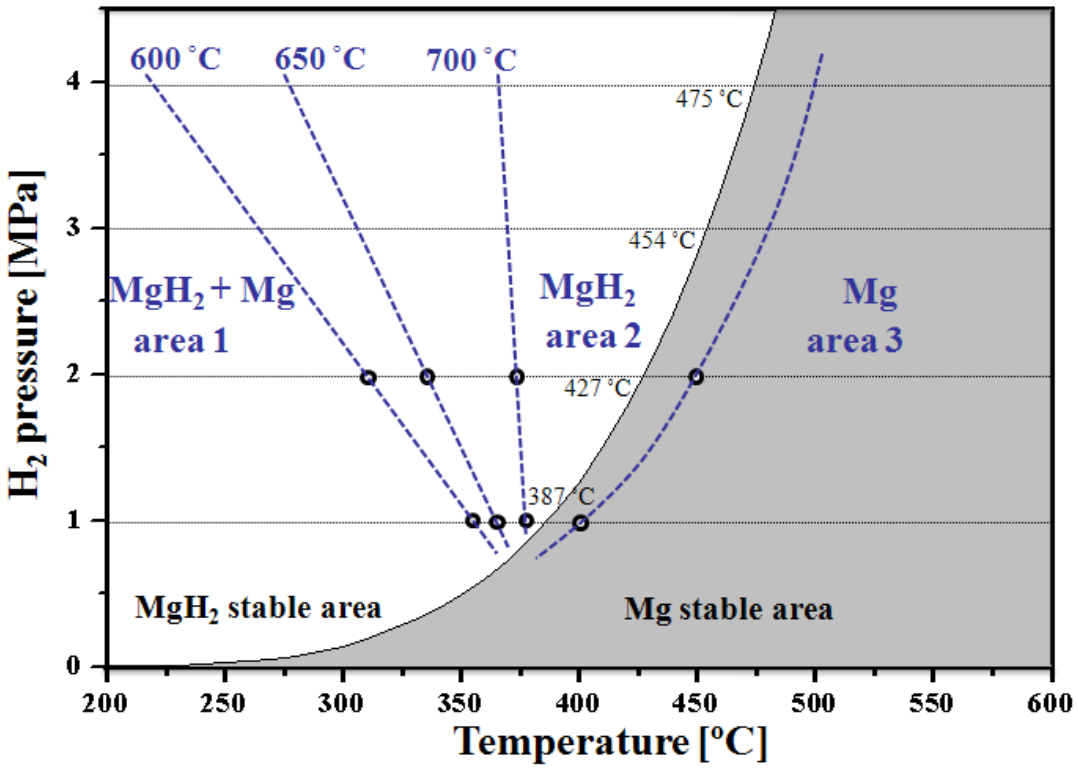

Figure 3. As-proposed boundaries for separating the high-purity MgH_2 production area and low-purity MgH_2 production area with evaporation temperatures of 600, 650, and 700 °C, as well as the experimentally measured boundary for the thermodynamically MgH_2 and Mg stable areas, in the *P-T* diagram of MgH_2. The boundary temperatures are based on the XRD composition analysis in Figure 2, which are the same with those blue lines in Figure 1. The white area shows the theoretically MgH_2 stable area, and the shadowed denotes the Mg stable area.

Figure 4

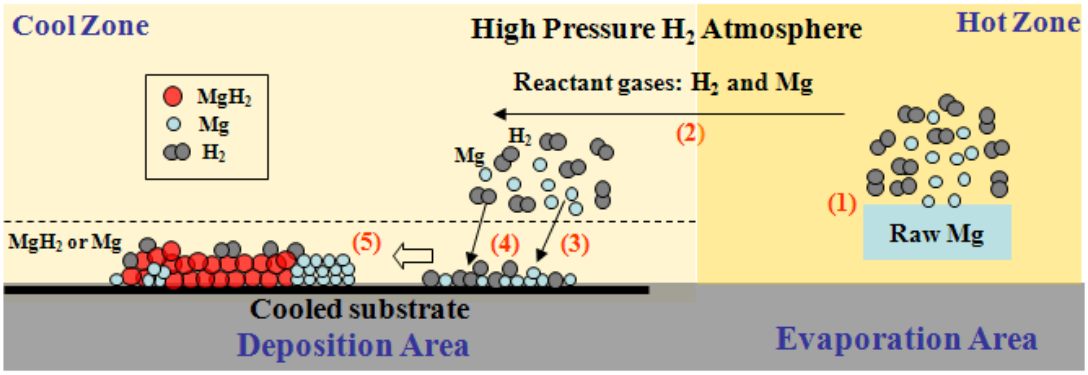

Figure 4. Sequence of steps in the HCVD process.

(1) Evaporation of raw Mg under high-pressure H_2 atmosphere in the hot region.

(2) Transfer of Mg gas by natural convection and diffusion of H_2 induced by the temperature gradient from the hot zone to the cool zone.

(3) Adsorption and condensation of Mg gas on the surface of the cooled substrate or the already formed deposits.

(4) Adsorption and dissociation of H_2 molecules on the surface of the cooled substrates or the already formed deposits.

(5) Formation of MgH_2 by the hydrogenation of the adsorbed and solidified Mg on the substrate at temperatures below the dissociation temperature of MgH_2 under a certain H_2 pressure. Above the dissociation temperature, only metallic Mg is formed. At very low deposition temperatures, the hydrogenation rate for the solidified Mg is slow, and the deposit contains un-hydrogenated Mg.

Figure 5

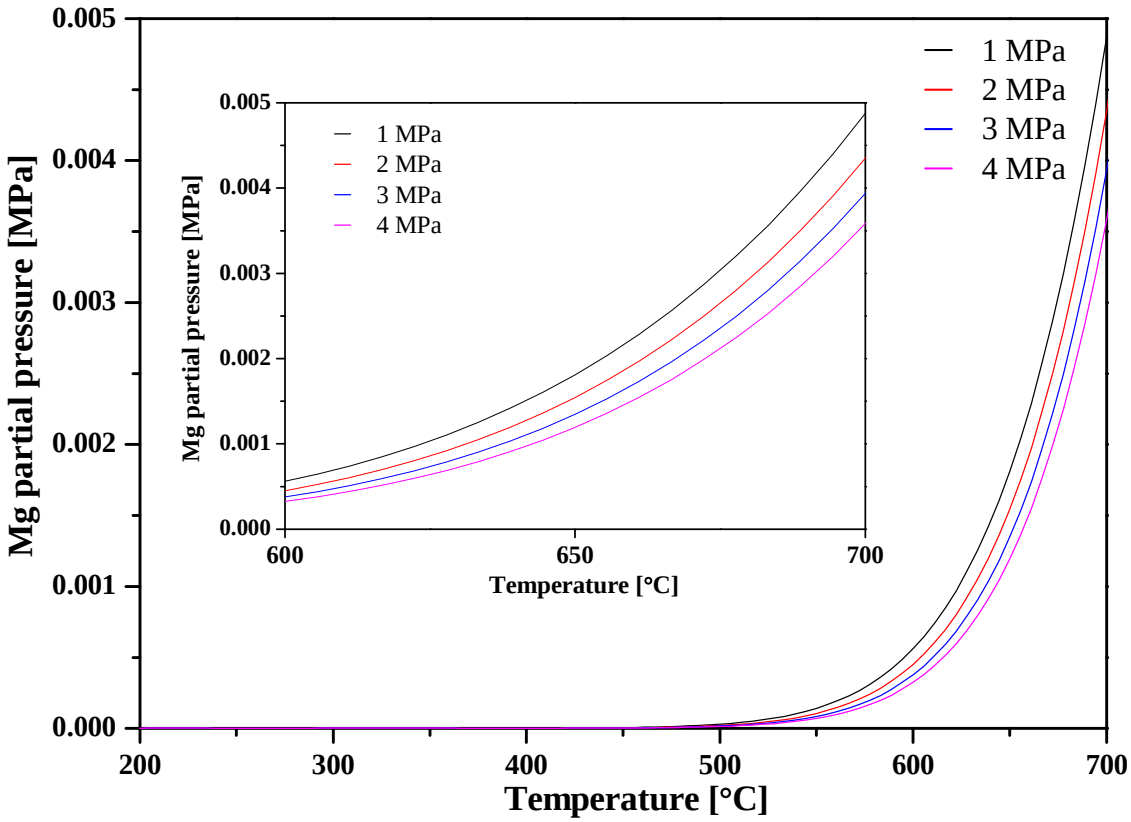

Figure 5. Equilibrium Mg gas partial pressure at different H_2 pressures (1, 2, 3, and 4 MPa) as a function of temperature. Inside shows an enlarged one ranging from 600 to 700 ºC.

Figure 6

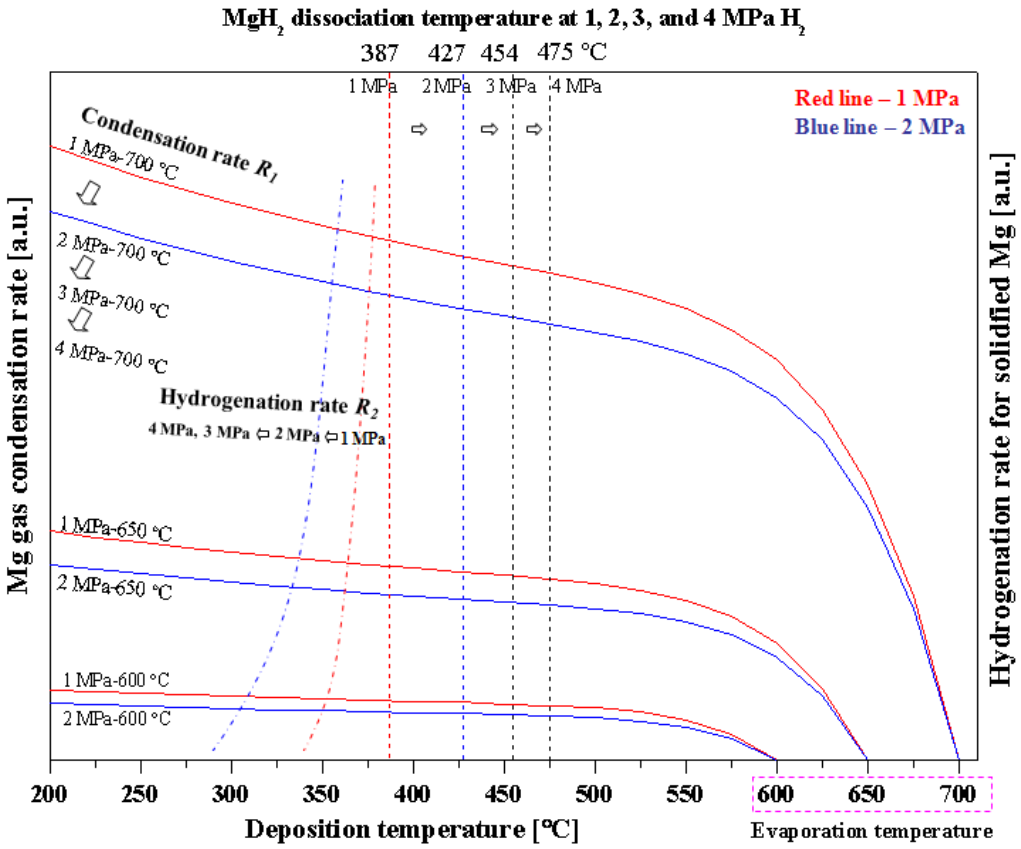

Figure 6. Calculated condensation rate for Mg gas as a function of deposition temperature under 1 and 2 MPa H_2 with evaporation temperatures of 600, 650, and 700 ˚C (Solid lines). As-proposed hydrogenation rates for the solidified Mg as a function of deposition temperature under 1 and 2 MPa H_2 are plotted in the dashed-dotted lines; the hydrogenation rate curves were plotted on the basis of the results of sample distribution obtained with a heating time of 4 h, as shown in Figures 1, 2, and 3. The dashed lines indicate the theoretical dissociation temperatures at different H_2 pressures. A thorough explanation of Figure 6 is shown in Figure S4 in the Supporting Information.